Steel and Composite Structures, *Vol. 35, No. 6 (2020) 739-752*
DOI: https://doi.org/10.12989/scs.2020.35.6.739

Full-range plasticity of novel high-performance low-cost stainless steel QN1803

Yiyi Zhou[1], Kim Eng Chouery[2], Jiang-Yue Xie[2], Zhan Shu[1] and Liang-Jiu Jia*[2]

[1]Department of Structural Engineering, School of Civil Engineering and Architecture, Changzhou Institute of Technology, 213000, China
[2]Department of Disaster Mitigation for Structures, College of Civil Engineering, Tongji University, Siping Road, Tongji University, Shanghai, 200092, China

(*Received February 15, 2020, Revised May 13, 2020, Accepted May 20, 2020*)

Abstract. This paper aims to investigate cyclic plasticity of a new type of high-performance austenitic stainless steel with both high strength and high ductility. The new stainless steel termed as QN1803 has high nitrogen and low nickel, which leads to reduction of cost ranging from 15% to 20%. Another virtue of the new material is its high initial yield strength and tensile strength. Its initial yield strength can be 40% to 50% higher than conventional stainless steel S30408. Elongation of QN1803 can also achieve approximately 50%, which is equivalent to the conventional one. QN1803 also has a corrosion resistance as good as that of S30408. In this paper, both experimental and numerical studies on the new material were conducted. Full-range true stress-true strain relationships under both monotonic and cyclic loading were obtained. A cyclic plasticity model based on the Chaboche model was developed, where a memory surface was newly added and the isotropic hardening rule was modified. A user-defined material subroutine was written, and the proposed cyclic plasticity model can well evaluate full-range hysteretic properties of the material under various loading histories.

Keywords: Chaboche model; memory surface; cyclic plasticity; high strength; stainless steel QN1803

1. Introduction

Advancement of civil engineering relies on development of new materials and new mechanics. Stainless steel has become more and more appealing to civil engineers for their virtues over conventional structural steel, e.g., high corrosion resistance, high ductility and toughness. Due to relative high cost of the material, it is commonly employed in some non-structural parts of a building, such as roofs and curtain wall systems. In some marine environment, it is also employed as structural members to avoid corrosion (Wang *et al.* 2019, Cai and Young 2018, 2019, Yousefi *et al.* 2017, 2018, Zhao *et al.* 2015). Generally, application of stainless steel in structural engineering is still limited, which is mainly due to consideration of high cost of stainless steel.

Recently, a new type of high-performance stainless steel with both high strength and high ductility was developed by a Chinese company. The new austenitic stainless steel termed as QN1803 employs a new metallurgical technology, which has high nitrogen and low nickel as shown in Table 1. Because of low nickel content, the material cost can be greatly reduced. The new technology can significantly reduce the cost by 15% to 20% compared with conventional S30408 stainless steel. The new material also has a high initial yield strength and tensile strength, where the initial yield strength is 40% to 50% higher than that of conventional S30408. The nominal yield strength of S30408 is 205 MPa, and the one of QN1803 is 440 MPa in this study. According to the definition of structural steel, steel with a yield strength beyond 420 MPa can be classified as high strength steel. Thus, QN1803 is a type of high strength stainless steel. It can be found that QN1803 shares similar properties with that of EN1.4162 as listed in Table 1 (Theofanous and Gardner 2009), which also has a high yield strength of around twice of the S30408, while has a price around 50% of S30408. The new material also has comparable ductility as conventional stainless steel, and its elongation can achieve approximately 50%. Corrosion resistance of QN1803 can be as good as that of S30408, and sometimes can be better than the latter. For example, cold-formed members using QN1803 has a higher pitting corrosion resistance than that of S30408. For aforementioned virtues, the new material has a great potential in civil engineering, such as roof systems, curtain wall systems and even structural members. Before application of the new material, it is necessary to obtain its constitutive relationship under monotonic loading. Meanwhile, cyclic plasticity of the material is also important for structural engineers when seismic loading is concerned.

A number of studies on monotonic stress-strain relationship of stainless steel were conducted (Arrayago *et al.* 2015), where mainly the Ramberg-Osgood model (Ramberg and Osgood 1943) was employed. It was found that the original Ramberg-Osgood model cannot capture full-range true stress-true strain relationship of stainless steel, and a number of studies two-stage (Gardner and

*Corresponding author, Ph.D.
E-mail: lj_jia@tongji.edu.cn

http://www.techno-press.org/?journal=scs&subpage=8
ISSN: 1229-9367 (Print), 1598-6233 (Online)

Table 1 Chemical composition of QN1803 stainless steel

Material	Chemical Composition (Weight %)									
	C	Si	Mn	P	S	Cr	Ni	Mo	Cu	N
QN1803	≤0.1	≤1.0	4.0-8.0	≤0.05	≤0.005	18.1-20.0	2.0-3.5	≤0.3	≥1.5	≤0.3
S30408	0.04	0.4	1.02	0.035	0.004	18.1	8.02	0.02	0.1	0.045
EN1.4162	0.025	0.8	4.99	0.02	0.001	21.64	1.5	0.3	0.31	0.209

Ashraf 2006, Mirambell and Real 2000, Rasmussen 2003), three-stage (Quach *et al*. 2008) and multistage (Hradil *et al.* 2013) Ramberg-Osgood models were thus developed. However, most of studies were focused on full-range engineering stress-engineering strain relationship but not true stress-true strain one (Jia *et al.* 2016, Jia and Kuwamura 2014).

Monotonic and cyclic plasticity of ductile metal has been extensively investigated, e.g., Chen *et al*. 2018, Wang *et al*. 2018, Hu and Shi 2016, Dundu 2018, Gao *et al.* 2018, Huang and Young 2017, Xiang *et al*. 2018. However, most of ductile metals have an elongation less than 30%, while elongation of the new stainless steel investigated in this study can reach as much as more than 50%. In addition, most of previous studies were focused on small plastic strain ranges, e.g., less than 5%. For structures in regions with a high seismic risk, full-range cyclic plasticity of a material is of interest. Structures can fail due to ductile fracture or ultra-low-cycle fatigue failure in a limited number of extremely large plastic strain ranges (Ge and Kang 2014, Jia 2014, Jia *et al*. 2016, Jia and Kuwamura 2014, 2015, Kang *et al.* 2015, Liao *et al*. 2015). Under this circumstance, strain concentration can be significant, and the maximum local true strain can reach as much as 100%. Up till now, only several studies were conducted for cyclic plasticity of stainless steel within small plastic strain ranges (Wang *et al.* 2014, Yin *et al*. 2019), and no study has been found for the new stainless steel QN1803. This material has a high potential to be employed in practice for its superior mechanical properties and low cost, especially in thin-walled structures. To stimulate its application in structural engineering, it is necessary to first understand and well evaluate its monotonic and cyclic plasticity.

2. Scope of this study

This paper aims to propose a model to well describe both monotonic and cyclic plasticity of the newly developed QN1803 stainless steel. To obtain full-range constitutive relationship of the material under monotonic loading, post-necking modification is necessary. In this paper, two post-necking modification methods were investigated and compared to obtain full-range true stress-true strain data till fracture. A two-parameter and a three-parameter function describing full-range constitutive relationship was respectively proposed. A cyclic plasticity model with a memory surface was developed to describe cyclic plasticity of QN1803 under full-range cyclic loading. A user-defined material subroutine was also written using Fortran to implement the newly-developed cyclic plasticity model. Both experimental and numerical studies were conducted to investigate cyclic plasticity of QN1803. For the experiments, compact specimens were designed under various loading histories, which can cover a variety of loading patterns and strain ranges. A simple method to calibrate the model parameters was also given. Through comparison of the experimental and numerical results, validity of the proposed cyclic plasticity model and parameter calibration method was proved. The proposed plasticity model can be further employed to many other metallic materials, especially for ones with high ductility.

3. Full-range monotonic true stress-true strain

3.1 Post-necking modification methods

This paper aims to describe full-range cyclic plasticity of the new high-performance stainless steel QN1803. In fact, it is not so easy to obtain full-range true stress-true strain data till fracture using a monotonic tension coupon test. The main challenge is a triaxial stress state of the coupon after necking initiation. Before necking initiation, the stress state of a material within the gage length is uniaxial tension, and this assumption doesn't hold for the post-necking stage. Thus, a post-necking modification method is required to obtain full-range true stress-true strain till fracture. Several studies have been done to solve the above problem. Bridgman (1952) proposed a theoretical method to obtain the post-necking true stress-true strain, while it requires accurate measurement of geometrical dimensions of the necked region, which is difficult for engineers. In fact, the cross section under post-necking stage can become elliptical, which also makes it more difficult to obtain an accurate result. Several methods using a combination of both numerical and experimental tools are proposed, and it is required to assume a monotonic hardening function of the post-necking stage. In this paper, two methods are employed, i.e., the weighted average (WA) method (Jia and Kuwamura 2014b) and the power law tangent (PLT) method (Jia *et al*. 2016) are both employed in this study.

It is widely accepted that necking generally occurs when the true stress is equal to tangent modulus of a true stress-true strain curve. The WA method postulates that the post-necking tangent modulus follows a linear function, and true stress can be given as follows

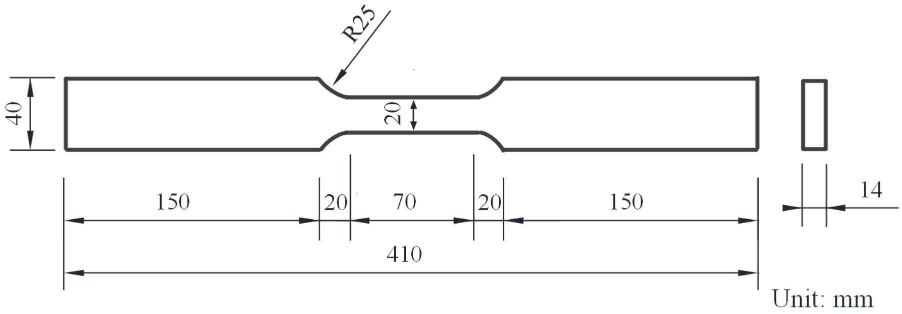

Fig. 1 Configuration of tension coupon

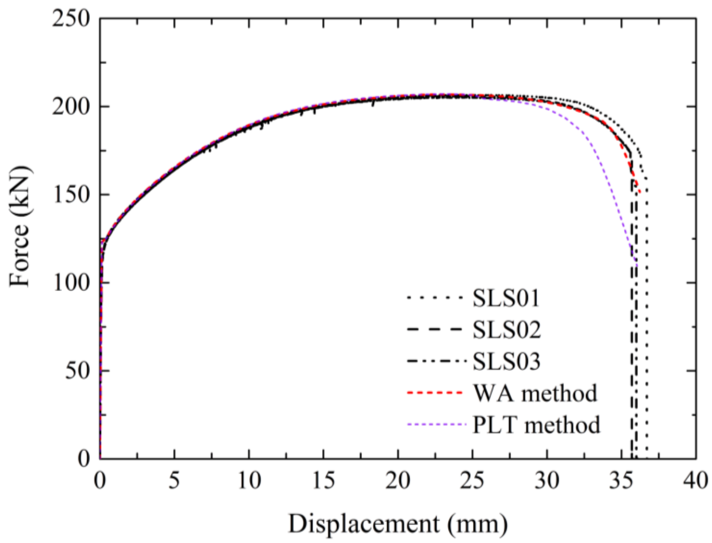

Fig. 2 Comparison of load-displacement curves of two post-necking true stress-true strain modification methods

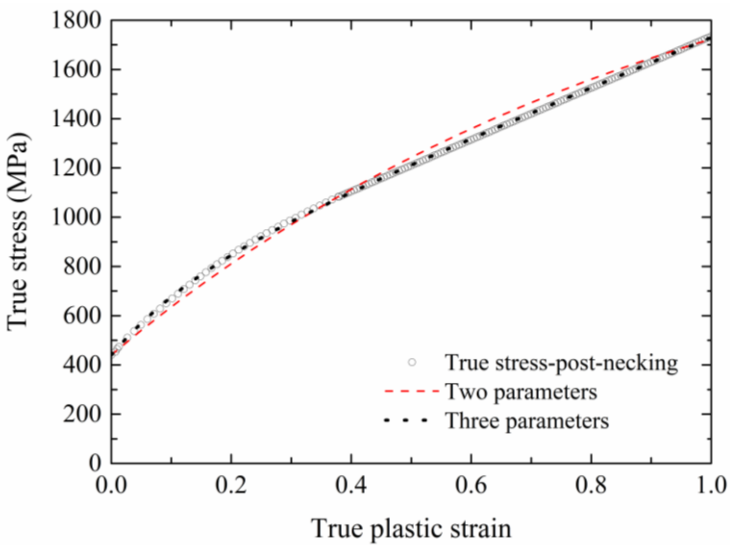

Fig. 3 Full-range monotonic true stress-true strain relationship of QN1803 stainless steel

$$\sigma = \sigma_{neck} + w \cdot \sigma_{neck} (\varepsilon - \varepsilon_{neck}) \quad (1)$$

where σ_{neck} and ε_{neck} are true stress and true strain when necking initiation occurs, respectively; w is a weight factor of the WA method.

Table 2 Mechanical properties of QN1803 stainless steel

Mechanical Properties						Post-necking modification parameters	
Yield stress	Tensile strength	Elongation	ε_{neck}	σ_{neck}	E	w	n
(MPa)	(MPa)	(%)	(%)	(MPa)	(MPa)		
440	737	71.3	38.0	1083	1.9×10^5	0.97	1.0

Notes: ε_{neck} and σ_{neck} are the true strain and true stress when necking initiates, respectively, E is Young's modulus. w and n are the parameters of the weighted average method and power law tangent method, respectively

The PLT method assumes that the true stress-true strain relationship of a material follows the power law given in the following formula

$$\sigma = \left(\frac{\sigma_{neck}}{\varepsilon_{neck}^{\varepsilon_{neck}}} \right) \varepsilon^{\varepsilon_{neck}} \quad (2)$$

The above formation can ensure that the true stress while necking occurs is equal to σ_{neck}. The PLT method also postulates that an upper bound of true stress follow a linear function, and the method can be expressed by the following equation

$$\sigma = \sigma_{neck}[w_1(1+\varepsilon-\varepsilon_{neck}) + (1-w_1)\left(\frac{\varepsilon^{\varepsilon_{neck}}}{\varepsilon_{neck}^{\varepsilon_{neck}}} \right)] \quad (3)$$

where w_1 is a weight factor of the PLT method. This method has also been employed for structural steel by other researchers (Ge *et al.* 2018).

3.2 Functions of full-range monotonic true stress-true strain

Three coupons with configuration shown in Fig. 1 were manufactured and pulled to rupture using an MTS testing machine. The configuration of coupons was designed based on the gauge length of the extensometer, which is 50 mm in this study, and the filleting radius is determined according to the specification, requiring a radius no less than 20 mm (GB/T 228.1-2010). Experimental results and corresponding numerical results using full-range true stress-true strain data with the aforementioned two post-necking methods are compared in Fig. 2. From the figure, it was found that the WA method can give a good evaluation of the stress-strain relationship of QN1803 stainless steel, while the PLT method cannot well describe the stress-strain relationship at the post-necking stage. This is mainly for the fact that the PLT method has an exponential expression, which will lead to no strain hardening at large strain range. The PLT method can underestimate the post-necking true stress of QN1803, and the necking deformation can be overestimated after necking initiates.

The load-displacement curves using full-range true stress-true strain data obtained by the two methods are compared in Fig. 2, indicates that the PLT method underestimates the ductility of the material due to premature necking of the tension coupon. Mechanical material properties of QN1803 stainless steel are given in Table 2, and corresponding material parameters of the two aforementioned post-necking modification methods are also listed in the table. The Young's modulus is about 1.9×10^5 MPa. Yield strength can reach 440 MPa, and tensile strength is 737 MPa. The yield to tensile strength of the new stainless steel QN1803 is 0.60, which is much less than 0.85. This indicates that the material has a large residual strength after yielding, which is favorable from viewpoint of ductile design. This also indicates a high strain hardening effect, which may lead to high requirement of connected members during structural design. Elongation of the coupons in this study can reach as much as 71.3%, where the uniform elongation before necking is 38.0%. Commonly, necking is deemed to initiate when the peak load is achieved, and the elongation of the material till the tensile strength is the uniform one, which is 38% for the QN1803 tested in this study. These values are much larger than most structural steel, indicating good ductility and energy dissipation capacity of the base metal. To facilitate application of the new material, two-parameter and three-parameter formulae to describe full-range true stress-true strain data till rupture under monotonic tension are given as follows

$$\sigma = \sigma_{y0} + a_1[1-\mathbf{exp}(-b_1\cdot\varepsilon_{eq})] = 440 + 2003[1-\mathbf{exp}(-1.02\varepsilon_{eq})] \quad (4)$$

$$\sigma = \sigma_{y0} + a_2[1-\mathbf{exp}(-b_2\cdot\varepsilon_{eq})] + K_m\cdot\varepsilon_{eq} = 440 + 270\times[1-\mathbf{exp}(-6.83\varepsilon_{eq})] + 1020\varepsilon_{eq} \quad (5)$$

Since Eqs. (4) and (5) are obtained based on test results of the three coupons employed in this study, more experimental results are required to further validate the parameters of the two formulae, where a_1 and b_1 are material constants of the two-parameter formula, and a_2, b_2 and K_m three-parameter ones. Full-range true stress-true strain data given by Eqs. (4) and (5) are compared with the one using the WA method in Fig. 3, indicating good accuracy of the two-parameter and three-parameter formulae. It can also be found that the three-parameter formula gives almost the same result of the WA method, which is a bit better than that of the two-parameter one. Both of the two formulae can be employed to describe full-range true stress-true strain data of QN1803 stainless steel under monotonic uniaxial loading.

4. Introduction of combined hardening models with/without a memory surface

4.1 Yield function and flow rule

Yield function describes the condition when a material yields. For ductile metal, commonly the Mises yield function is employed both for its accuracy and mathematical formation, though it can overestimate yield stress under shear-dominant loading conditions. For the combined hardening Chaboche model, there are both isotropic and kinematic hardening (KH) components. The yield function can be generally written as

$$f = \sqrt{\frac{3}{2}(\mathbf{S}-\boldsymbol{\alpha}):(\mathbf{S}-\boldsymbol{\alpha})} - (\sigma_{y0} + R) = 0 \tag{6}$$

where $\mathbf{S}$ is the deviatoric stress tensor; $\boldsymbol{\alpha}$ is the total backstress tensor, which gives movement of center of the yield surface; σ_{y0} is initial yield strength; R is an isotropic hardening (IH) component, indicating increase in size of the yield surface. The flow rule describes how plastic strain increases. For ductile metal, the associated flow rule is generally employed, and it assumes that the plastic potential function is identical to yield function.

4.2 Combined hardening rule

A hardening rule describes how the yield surface evolves under the post-yielding stage. For ductile metals following the Mises yield function and the associated flow rule, formation of the backstress proposed by Armstrong and Frederick (1966) can be employed

$$\mathrm{d}\boldsymbol{\alpha} = \frac{2}{3}C_0 \mathrm{d}\boldsymbol{\varepsilon}_\mathbf{p} - \gamma \cdot \boldsymbol{\alpha} \cdot \mathrm{d}\varepsilon_{eq} \tag{7}$$

where C_0 / γ gives the stabilized value of KH stress; γ gives the hardening rate of KH stress; $\mathrm{d}\boldsymbol{\varepsilon}_\mathbf{p}$ is increment of the plastic strain tensor; $\mathrm{d}\varepsilon_{eq}$ is incremental equivalent plastic strain. It can be found that the Armstrong-Frederick rule will reduce to the Prager hardening rule when γ is equal to zero

$$\mathrm{d}\boldsymbol{\alpha} = \frac{2}{3}C_0 \mathrm{d}\boldsymbol{\varepsilon}_\mathbf{p} = C'_0 \mathrm{d}\boldsymbol{\varepsilon}_\mathbf{p} \tag{8}$$

For a uniaxial stress state, expression of the backstress in incremental form shown in Eq. (7) can be rewritten as

$$\boldsymbol{\alpha} = \begin{cases} \frac{C_0}{\gamma}[1\text{-}\mathbf{exp}(\text{-}\gamma\,\boldsymbol{\varepsilon}_\mathbf{p})] & \text{when } \gamma \neq 0 \\ C_0\,\boldsymbol{\varepsilon}_\mathbf{p} & \text{when } \gamma = 0 \end{cases} \tag{9}$$

It can found from Eq. (9) that the backstress $\boldsymbol{\alpha}$ follows an exponential function, indicating that it will converge to a limit value of C_0 / γ when γ is not equal to zero. The Armstrong-Frederick rule with only a single backstress is generalized by Chaboche et al. (Chaboche and Dang 1979, Chaboche and Rousselier 1983), who introduced several backstresses each with different hardening parameters to describe different hardening rates at full strain range. The generalized Armstrong-Frederick rule is also termed as Chaboche model, which gives much better evaluation of cyclic plasticity of metal than that of the Armstrong-Frederick rule for some ductile metal. There can be several backstresses in the generalized Armstrong-Frederick rule (Chaboche and Dang 1979, Chaboche and Rousselier 1983)

$$\boldsymbol{\alpha} = \sum_i^n \boldsymbol{\alpha}_i\ ;\ \ \mathrm{d}\boldsymbol{\alpha}_i = \frac{2}{3}C_i \mathrm{d}\boldsymbol{\varepsilon}_\mathbf{p} - \gamma_i \cdot \boldsymbol{\alpha}_i \cdot \mathrm{d}\varepsilon_{eq} \tag{10}$$

where $\boldsymbol{\alpha}_i$ is the i-th backstress; n is total number of backstresses; C_i / γ_i gives the stabilized value of the i-th backstress at large strain range; γ_i describes hardening rate of KH component of the i-th backstress. Different backstresses can have different hardening rates, which thus can lead to better description of cyclic plasticity of ductile metal at various strain ranges. For example, there can be two backstresses. One is expected to determine large strain range, and the other one together with the first one to define small strain range.

For the combined hardening model, there is also an IH component, R. Incremental form of the IH rule (Jia and Kuwamura 2014 a) is given as

$$\mathrm{d}R = k(Q_\infty - R)\mathrm{d}\varepsilon_{eq} \tag{11}$$

where $\mathrm{d}R$ represents incremental increase of size of the yield surface; k gives hardening rate of the IH rule; Q_∞ gives stabilized value of R commonly at a large strain level. For a uniaxial stress state, the IH component can be expressed as an exponential function, which is almost the same as expression of the backstress in the Armstrong-Frederick rule when γ is not equal to zero

$$R = Q_\infty[1 - \mathbf{exp}(-k \cdot \varepsilon_{eq})] \tag{12}$$

For the combined hardening model (termed as Chaboche model in this paper), commonly there are two or three backstresses, where commonly one of them has a linear formation to describe stress-strain relationship at large plastic strain range.

In this paper, the IH rule shown in Eq. (12) was revised to obtain a better evaluation of cyclic plasticity of the new material. An additional linear function was added in Eq. (12) in the proposed plasticity model with a memory surface. The IH hardening rules can thus be written as

$$\mathrm{d}R = \mathrm{d}R_1 + \mathrm{d}R_2 \tag{13}$$

$$\begin{aligned} R_1 &= Q_\infty[1 - \exp(-k\varepsilon_{eq})] \\ R_2 &= K_c \varepsilon_{eq} \end{aligned} \tag{14}$$

where R_1 and R_2 are two IH hardening components, K_c is post-yielding hardening modulus of the second IH component, R_2. Without the linear item, the IH component of the original Chaboche model will converge to a limit value of Q_∞, and this will underestimate the hardening modulus of the material at large plastic ranges, leading to premature necking prediction.

4.3 Memory surface

It has been found that stress can achieve a stabilized value after several constant-amplitude loading cycles, and hardening will occur again when the previous peak amplitude is exceeded. To describe this effect, memory

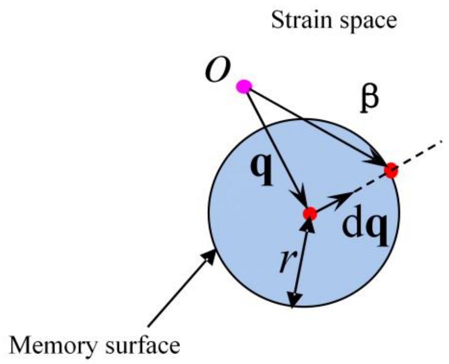

Fig. 4 Memory surface in strain space

surface is necessary to memorize loading history. Ohno (1982) proposes a formation for a memory surface in strain space as illustrated in Fig. 4, which is employed in this study. A memory surface, g_ε, is defined (Ohno 1982) as follows

$$g_\varepsilon = \sqrt{\frac{2}{3}(\boldsymbol{\varepsilon}_\mathbf{p} - \mathbf{q}):(\boldsymbol{\varepsilon}_\mathbf{p} - \mathbf{q})} - r = 0 \tag{15}$$

where $\mathbf{q}$ and r are center and radius of the memory surface, respectively.

Evolution rule of the memory surface is given as

$$\mathrm{d}\mathbf{q} = \mu(\boldsymbol{\varepsilon}_\mathbf{p} - \mathbf{q}) \tag{16}$$

where the initial value of $\mathbf{q}$ is zero.

Consistency condition of the surface, g_ε, leads to

$$\frac{\partial g_\varepsilon}{\partial \boldsymbol{\varepsilon}_\mathbf{p}}:\mathrm{d}\boldsymbol{\varepsilon}_\mathbf{p} + \frac{\partial g_\varepsilon}{\partial \mathbf{q}}:\mathrm{d}\mathbf{q} + \frac{\partial g_\varepsilon}{\partial r}\cdot \mathrm{d}r = 0 \tag{17}$$

One can obtain

$$\mu = \frac{2(\boldsymbol{\varepsilon}_\mathbf{p} - \mathbf{q}):\mathrm{d}\boldsymbol{\varepsilon}_\mathbf{p}}{3r^2} - \frac{\mathrm{d}r}{r} \tag{18}$$

Evolution rule of r is assumed to be

$$\mathrm{d}r = h\eta, \quad \eta = \frac{2(\boldsymbol{\varepsilon}_\mathbf{p} - \mathbf{q}):\mathrm{d}\boldsymbol{\varepsilon}_\mathbf{p}}{3r} \quad \text{when } \mathrm{d}R > 0 \tag{19}$$

where h is a parameter determining expanding rate of the memory surface, and r will increase only when dR is larger than zero. According to Eq. (19), there will be no IH if current strain state is within the memory surface or angle between current plastic strain increment and normal of the memory surface is larger than 90 degrees. With the above memory surface, stress stabilization phenomenon of metal under cyclic constant-amplitude loading can be captured. For a cyclic plasticity model without the memory surface, stress will continue increasing under cyclic constant-amplitude loading, which will overestimate stress under such loading histories.

5. Calibration of model parameters

Prediction accuracy of a plasticity model is significantly affected by corresponding parameter calibration method. For structural engineers, it will be straightforward if all parameters of cyclic plasticity models can be calibrated using only tension coupon test results. A method to determine cyclic plasticity model parameters using only tension coupon test results was proposed by one of the authors (Jia and Kuwamura 2014a) based on observation during fatigue tests (Kuhlmann-Wilsdorf and Laird 1979), and good evaluation accuracy was achieved. It was postulated that IH and KH components each takes half of hardening stress for structural steel and aluminum. For the Chaboche model, full-range true stress under monotonic loading can be expressed as

$$\sigma_i = \sigma_{y0} + R + \alpha \tag{20}$$

where σ_i is true stress after post-necking modification. By postulating that ratio of the IH one to total hardening stress is constant for full strain ranges, a variable β can be defined as illustrated in Fig. 5, and IH and KH stresses under monotonic loading can be determined as follows

$$R = \beta(\sigma_i - \sigma_{y0}) \tag{21}$$

$$\alpha = (1-\beta)(\sigma_i - \sigma_{y0}) \tag{22}$$

β is assumed to be a material constant, which can be calibrated based on comparison results of monotonic and cyclic tests. From Eqs. (21) and (22), it can be found that IH and KH functions can be easily obtained if value of β is known. According to Eq. (12), IH correlated parameters, Q_∞ and k, can be obtained based on a simple regression analysis. Likewise, KH correlated parameters, C_i and γ_i, can also be simply obtained based on a regression analysis. For the proposed plasticity model with two IH components, value of k is the same as that of γ_1, and value of Q_∞ is equal to C_1 / γ_1. K_c in Eq. (14) can be obtained by multiplying β and K_m in Eq. (5).

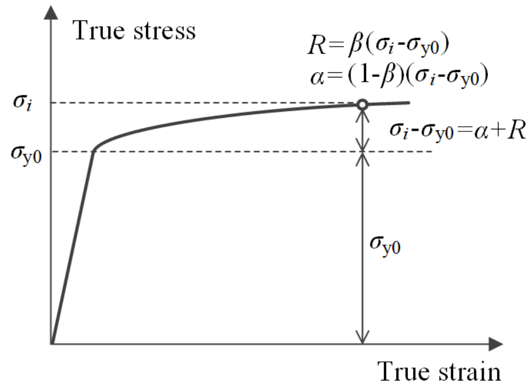

Fig. 5 Decomposition of isotropic and kinematic hardening stress in tensile stress-strain

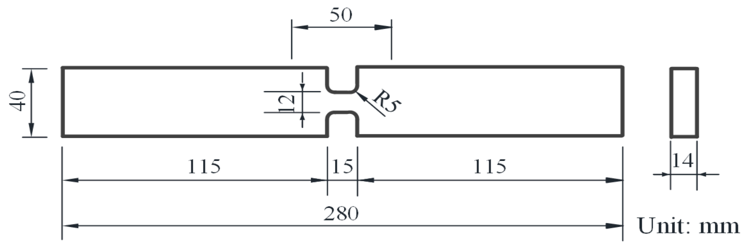

Fig. 6 Configuration of compact specimens under both monotonic and cyclic loadings

For structural steel and aluminum, it was found that the optimal value of β is close to 0.5. Based on comparison of monotonic and cyclic test results, an optimal value of 0.5 is obtained for QN1803 stainless steel, which is the same as those of structural steel and aluminum. The main reason may be that the cyclic hardening mechanism of these metals are basically the same, i.e., induced by crystal dislocation.

6. Experimental study

6.1 Configuration of specimens

Eight QN1803 stainless steel specimens with configuration shown in Fig. 6 were designed and manufactured. The configuration in the figure was designed by the authors to achieve cyclic large strain loading. A compact configuration was designed to avoid premature elasto-plastic buckling of the specimens under compression at large strain range. All specimens were cut from the same 14-mm thick stainless steel plate. The central segment has a length of 5 mm with a uniform cross-section to achieve a stress state close to uniaxial loading. The specimens were designed as compact as possible to avoid premature elastoplastic buckling under cyclic plastic loading. Width of the central minimum cross-section is 12 mm, which is close to the thickness to avoid premature out-of-plane buckling. The central segment with a small length of 5 mm has the same cross-sectional area to produce a stress state as uniform as possible. The compact configuration was determined to avoid premature buckling under compression. Three coupons as illustrated in Fig. 1 were manufactured and pulled to fracture. Coupon test results were employed to obtain parameters of the Chaboche model with a memory surface. Manufactured specimens are shown in Fig. 7, and the tests were conducted using an MTS testing machine under room temperature at a quasi-static speed of 0.01 mm/s. Capacity of the loading machine is 500 kN, and displacement capacity is ±75 mm. Specimens were clamped to the bottom loading head, and enforced displacement was applied to the top movable loading head. An extensometer with a gage length of 50 mm was employed to measure net deformation of the central segment as shown in Fig. 8. All the tests were controlled by displacement data of the extensometer. Specimens were tested under different loading histories as illustrated in Fig. 9. A tension test was employed to verify the maximum tensile displacement capacity and necking initiation point of the specimen, and a compression test was to obtain instant when global buckling of the specimen occurs. Based on test results of the above two specimens, cyclic loading histories covering various strain ranges can be designed while avoiding premature buckling of specimens under compression. Single full cycle loading history and five constant-amplitude cycles loading histories respectively shown in Figs. 9(c) and 9(d) were designed to investigate the stress stabilization effect under constant-amplitude cyclic loading. Two cycles pre- and post-necking loading histories respectively shown in Figs.

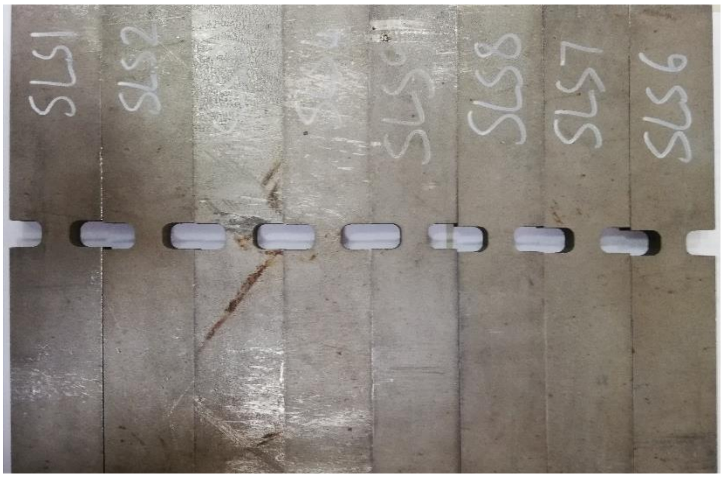

Fig. 7 Manufactured QN1803 specimens

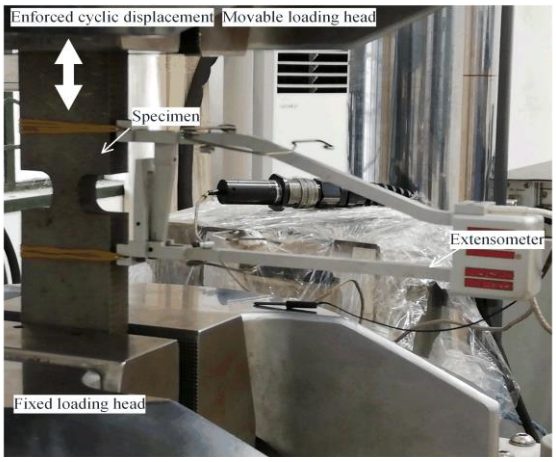

Fig. 8 Test setup of specimens

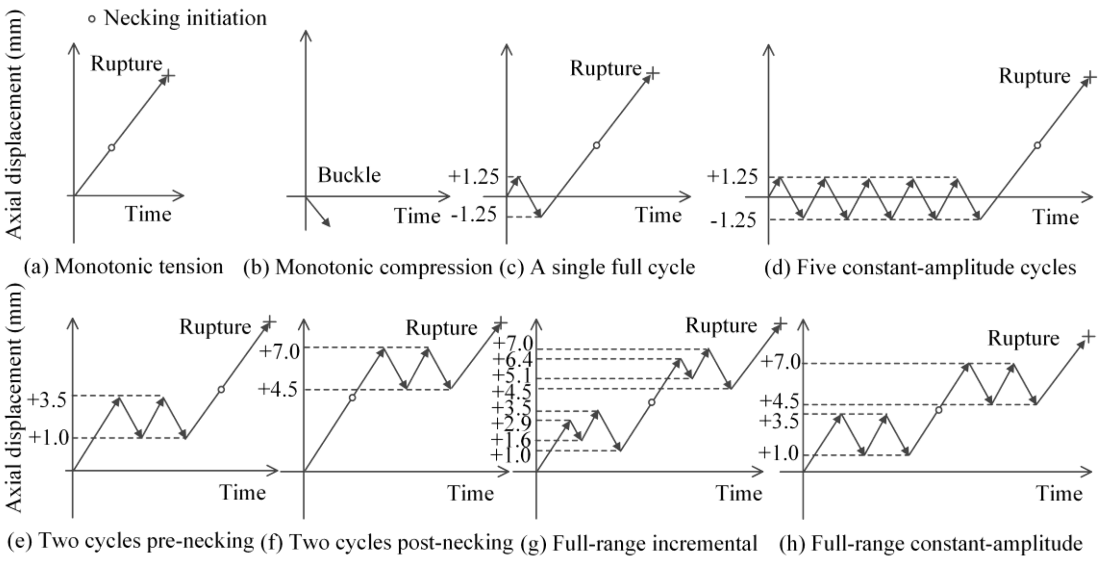

Fig. 9 Loading histories for specimens

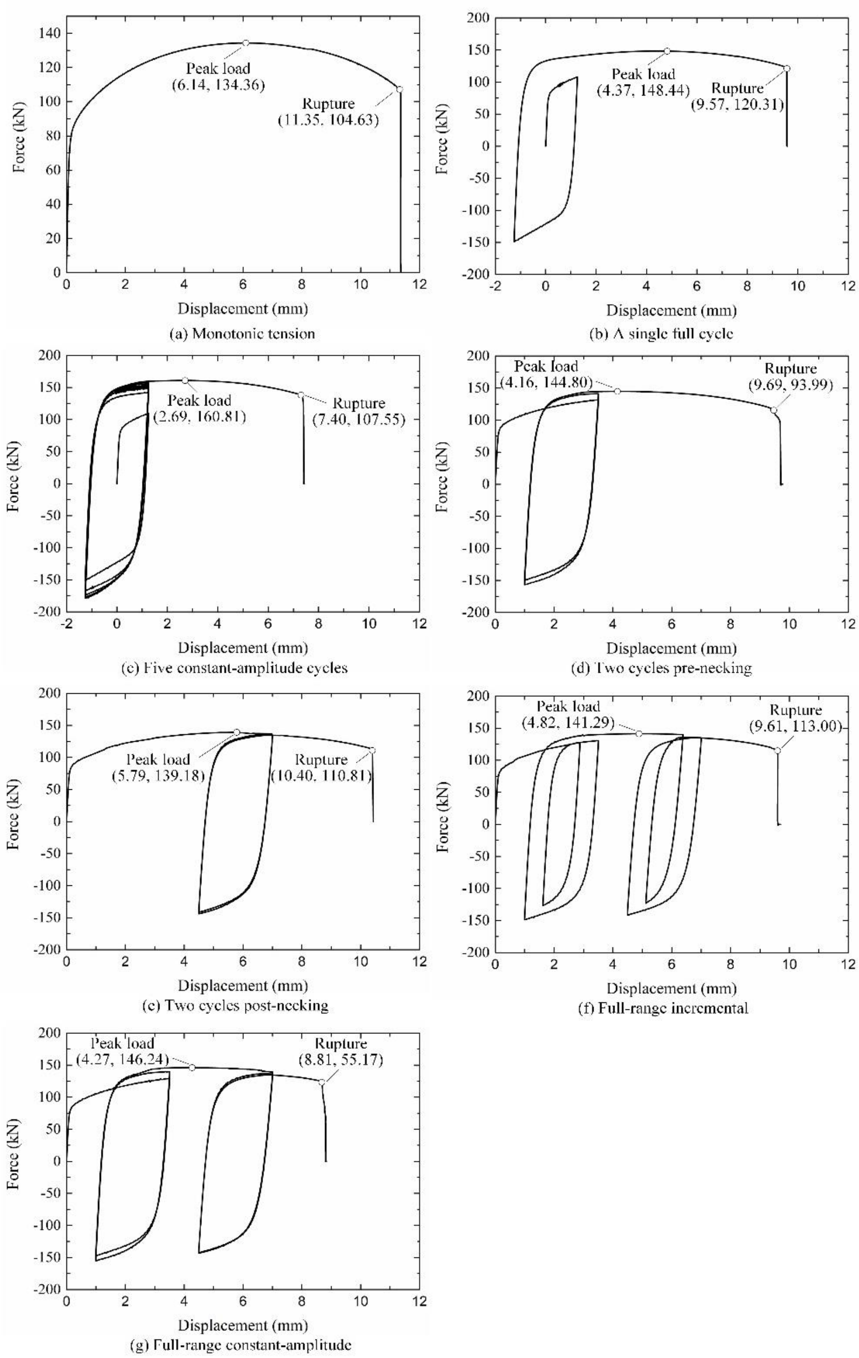

Fig. 10 Experimental results of specimens

9(e) and 9(f) were also designed to investigate cyclic plasticity of the material in strain ranges before and after necking initiation, where the necking initiation point under monotonic tension was also given in the figure. The last two loading histories, i.e., the full-range incremental and constant-amplitude loading histories respectively shown in Fig. 9(g) and 9(h), were designed investigate cyclic plasticity of the material in full strain range. Cyclic plasticity of QN1803 stainless steel can be investigated comprehensively based on the aforementioned experimental study and corresponding numerical one.

6.2 Experimental results

Experimental results of the specimens are shown in Fig. 10, where loads and displacement at peak and rupture points are also given. The load-displacement curves are compared since the stress state at the post-necking stage is not uniaxial. The stress and strain distribution of central uniform cross section is not uniform. From the figure, it can be found that cyclic loading can lead to premature necking initiation. Necking initiates at 2.69 mm for the five cycles constant-amplitude loading, while the one under monotonic

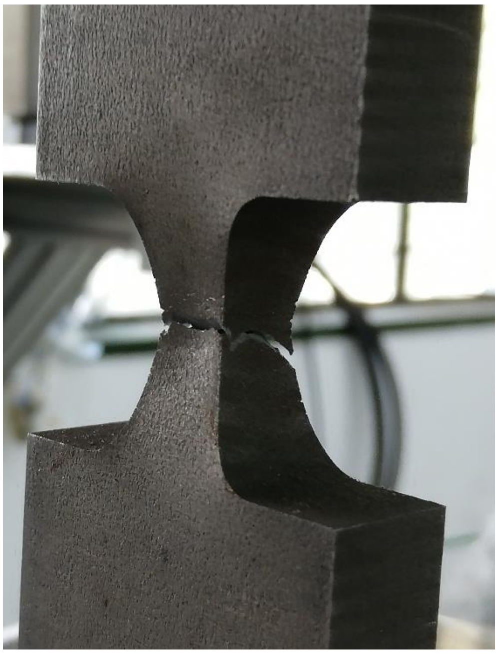

Fig. 11 Failure mode of specimens

Table 3 Calibrated model parameters of the plasticity models

Chaboche model	β	C_1 (MPa)	γ_1	C_2 (MPa)	γ_2	Q_∞ (MPa)	k	K_c (MPa)
With memory surface	0.5	922.73	6.83	510.35	0	135.05	6.83	510.35
Without memory surface	0.5	922.73	6.83	510.35	0	1001.5	1.02	

tension is 4.37 mm. The peak load of specimen under the five cycles constant-amplitude loading is also larger than the ones of the other specimens. In addition, pre-necking cyclic plastic straining can also lead to premature rupture of specimens, e.g., rupture displacement of the specimen under five cycles constant-amplitude loading is 7.40 mm, which is much less than the monotonic one, which is 9.57 mm. It is interesting to find that post-necking cyclic plastic straining can even increase rupture displacements of specimens, e.g., the one under two cycles post-necking has a rupture displacement of 10.40 mm. All specimens failed in a ductile failure mode as shown in Fig. 11 except for the monotonic compression one. Necking first initiates at middle of the specimens, and ductile rupture finally occurs.

7. Numerical study

7.1 Finite element modeling

A three-dimensional solid model as shown in Fig. 12 was established in ABAQUS (ABAQUS, 2013) to simulate cyclic plasticity of QN1803 stainless steel. A one-eighth model was employed considering symmetric boundary conditions of specimens. Element type C3D8R with a reduced integration scheme was employed for its accuracy and efficiency. Only portion within gage length of the extensometer was simulated. Symmetric boundary conditions were applied to the model as shown in Fig. 12(a), and mesh of the numerical model was shown in Fig. 12(b), where the central uniform part was meshed with fine elements considering strain concentration there. Enforced displacement was applied to top of the specimen. In this study, both the Chaboche models with and without the memory surface were employed in the above numerical study. The two plasticity models both employ a combined hardening rule, with both IH and KH rules. The only difference is that there is a memory surface in strain space for the proposed plasticity model. The one without a memory surface is available in ABAQUS, and the proposed plasticity model was implemented into software using a user-defined subroutine developed in Fortran. The user-defined subroutine is termed as VUMAT in ABAQUS, which employs an explicit integration scheme. The plasticity model parameters are all calibrated through monotonic coupon test results using the aforementioned method. Values of the calibrated plasticity model parameters are given in Table 3.

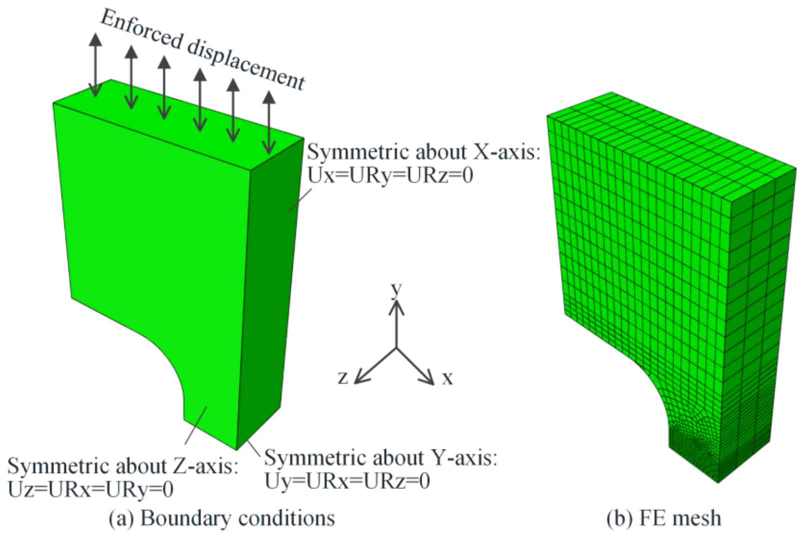

Fig. 12 Boundary conditions and FE mesh of specimens

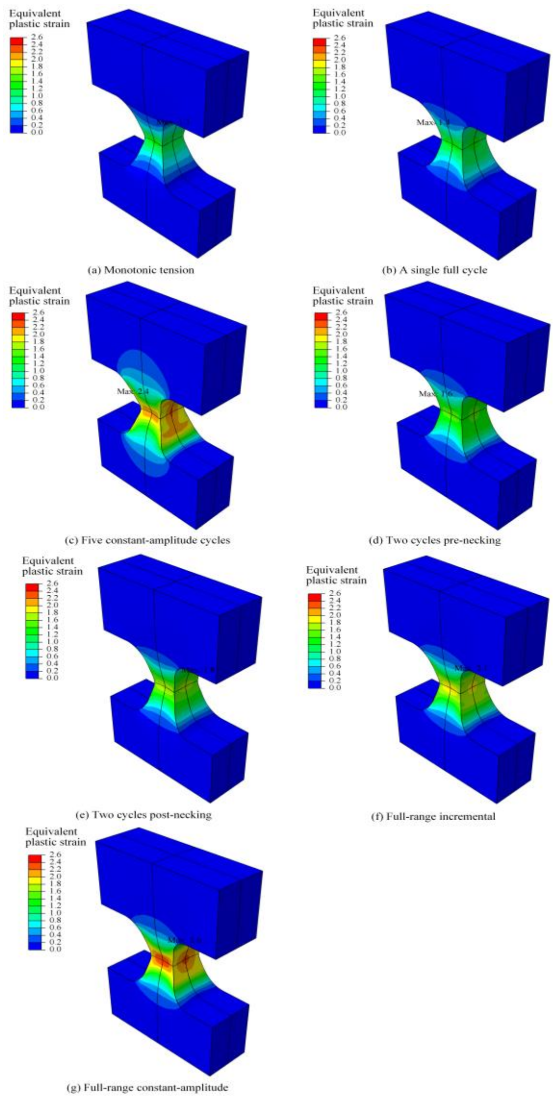

Fig. 13 Contour plots of equivalent plastic strain at instant of rupture

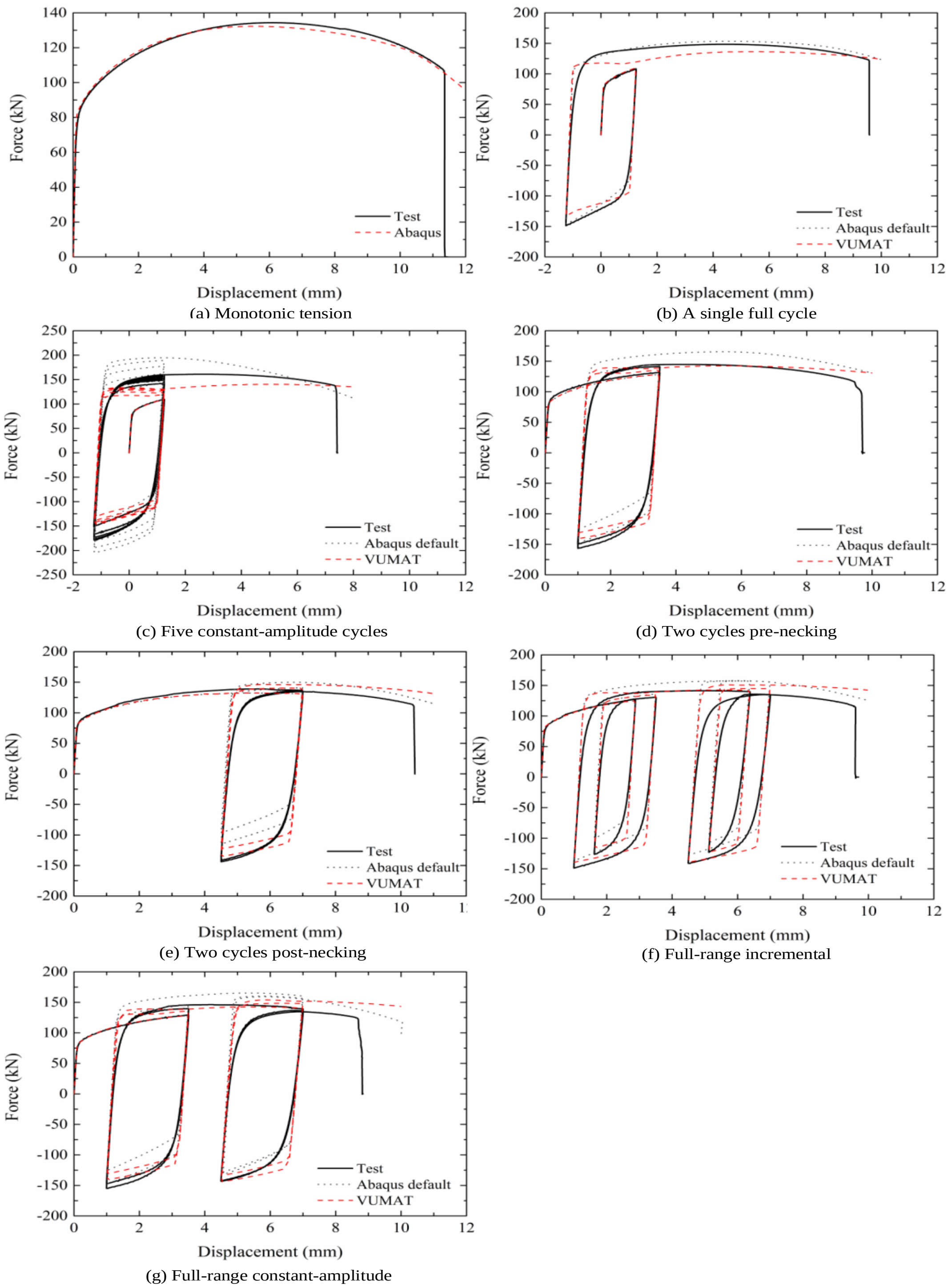

Fig. 14 Comparison of experimental and numerical results for specimens

7.2 Numerical results

Equivalent plastic strain contour plots obtained from the numerical simulation were given in Fig. 13, implying extremely large plastic strain. The maximum value can reach as much as 260% for specimen under the full range constant-amplitude loading, and the maximum equivalent plastic strain of specimen under monotonic tension is 130%. The elongation of the material is 71.3% in this study, and true strain at the necked region can be much larger.

Load-displacement curves obtained from the numerical simulation were compared with corresponding experimental results in Fig. 14, where “Abaqus default” denotes the Chaboche model without a memory surface, and VUMAT denotes the proposed model with a memory surface. Based on comparison results, following observations can be found:

(1) The Chaboche model without a memory surface can give a good evaluation result for the specimen under a single full cycle loading, which is even a bit better than the proposed model with a memory surface.

(2) For the specimen under five constant-amplitude cycles loading, the Chaboche model without a memory surface greatly overestimates cyclic hardening at both tensile and compressive sides during constant-amplitude loading stage, while predicting a premature necking initiation of the specimen. The Chaboche model with a memory surface can generally give a good evaluation result for the specimen.

(3) For the specimen under two cycles pre- and post-necking loadings, the Chaboche model without a memory surface can overestimate stress at tensile side, while underestimate the one at compressive side. The Chaboche model with a memory surface can generally give a good evaluation result for the specimen.

(4) Similar conclusion to the ones under pre- and post-necking loadings can be obtained for the two specimens under full range cyclic loading histories.

It can also be found that the hardening moduli as the elasto-plastic transition zones are overestimated by the proposed model. The deviation is mainly correlated the calibration method for the cyclic plasticity model, where the model parameters are calibrated using monotonic tension coupon test results. The hardening modulus at the transition zone of the first loading cycle is much higher than those of the subsequent ones. This leads to overestimation of the VUMAT at the transition zones except the first half cycle.

8. Conclusions

A new austenitic stainless steel termed as QN1803 with high nitrogen and low nickel was recently invented, which leads to significant reduction of material cost by approximate 15% to 20%. In addition, the new material has high initial yield strength and tensile strength. This high-performance material has a high potential to be widely employed in many applications. In this study, an experimental study on cyclic plasticity of the new high-performance stainless steel QN1803 was conducted to investigate its full-range monotonic and hysteretic properties. A combined cyclic plasticity model with a new isotropic hardening (IH) rule was proposed, and a memory surface in strain space was also employed to simulate the new high-performance material. The newly developed plasticity model was implemented into ABAQUS using a user-defined subroutine. Numerical study was carried out to capture cyclic plasticity of the new material and verify validity of the newly proposed model. Based on experimental and numerical results, following conclusions can be made.

(1) For the new high-performance stainless steel QN1803, yield strength can reach 440 MPa and it has an elongation beyond 50% in this study, indicating QN1803 has high strength and good ductility. In addition, the yield to tensile strength ratio can be as low as 0.60, implying high strain hardening effect and a high post-yielding strength potential.

(2) Both two-parameter and three-parameter formulae were proposed for full-range true stress-true strain relationship of the material, and the three-parameter one with an exponential function and a linear one gives the best evaluation accuracy.

(3) The newly proposed plasticity model with a new IH rule and a memory surface in strain space can generally well simulate full-range cyclic plasticity of QN1803 stainless steel under various loading histories.

(4) The Chaboche model without a memory surface can greatly overestimate cyclic strain hardening effect under cyclic constant-amplitude loading and underestimate stress at reversal sides under some cyclic loading histories, e.g., cyclic incremental loading.

(5) Based on comparison between numerical and experimental results, ratio of the IH component to total post-yielding hardening stress, β, can be taken as 0.5 for QN1803 stainless steel.

Acknowledgements

This study is supported by National Natural Science Foundation of China (51678082), and support from the Fundamental Research Funds for the Central Universities is also greatly appreciated. Thanks also goes to Tsingshan Holding Group for providing the stainless steel QN1803 and Qiangchao Machinery Factory for fabrication.

References

Armstrong, P.J. and Frederick, C.C. (1966), “A mathematical representation of the multiaxial Bauschinger effect”, CEGB Rep. No. RD/B/N731, Central Electricity Generating Board, Berkeley, UK.

Arrayago, I., Real, E. and Gardner, L. (2015), “Description of stress–strain curves for stainless steel alloys”, *Mater. Design*, **87**, 540-552. DOI: 10.1016/j.matdes.2015.08.001.

Bridgman, P.W. (1952). "Studies in large plastic flow and fracture." McGraw-Hill, New York.

Cai, Y. and Young, B. (2018), “Bearing resistance design of stainless steel bolted connections at ambient and elevated temperatures”, *Steel Compos. Struct.*, **29**(2), 273-286. https://doi.org/10.12989/scs.2018.29.2.273

Cai, Y. and Young, B. (2019), “Experimental investigation of carbon steel and stainless steel bolted connections at different strain rates”, *Steel Compos. Struct.*, **30**(6), 551-565. https://doi.org/10.12989/scs.2019.30.6.551.

Chaboche, J.L. and Dang, V. (1979), “Modelization of the strain memory effect on the cyclic hardening of 316 stainless steel”, ONERA, TP no., 1979-109.

Chaboche, J.L. and Rousselier, G. (1983), “On the plastic and viscoplastic constitutive equations—Part II: application of internal variable concepts to the 316 stainless steel”, *J. Pressure Vessel Technol.*, **105**(2), 159-164. DOI: 10.1115/1.3264258

Chen, X., Chen X. and Chen, H. (2018), “Influence of stress level on uniaxial ratcheting effect and ratcheting strain rate in austenitic stainless steel Z2CND18.12N”, *Steel Compos. Struct.*, **27**(1), 89-94. https://doi.org/10.12989/scs.2018.27.1.089.

Dundu, M. (2018), “Evolution of stress–strain models of stainless steel in structural engineering applications”, *Constr. Build. Mater*., **165**, 413-423. DOI: 10.1016/j.conbuildmat. 2018. 01. 008.

Gao, X., Zhang, X., Liu, H., Chen, Z. and Li, H. (2018), “Residual mechanical properties of stainless steels S30408 and S31608 after fire exposure”, *Constr. Build. Mater*., **165**, 82-92. DOI: 10.1016/j.conbuildmat. 2018.01.020.

Gardner, L. and Ashraf, M. (2006), “Structural design for non-linear metallic materials”, *Eng. Struct*., **28**(6), 926-934. DOI: 10.1016/j.engstruct.2005.11.001.

GB/T 228.1 (2010), Metallic materials-Tensile testing-Part 1: Method of test at room temperature.

Ge, H.B. and Kang, L. (2014), “Ductile crack initiation and propagation in steel bridge piers subjected to random cyclic loading”, *Eng. Struct*., **59**, 809-820. DOI: 10.1016/j.engstruct.2013.12.006.

Hradil, P., Talja, A., Real, E., Mirambell, E. and Rossi, B. (2013), “Generalized multistage mechanical model for nonlinear metallic materials”, *Thin-Wall. Struct*., **63**, 63-69. DOI: 10.1016/j.tws.2012.10.006.

Hu, F., Shi, G. and Shi, Y. (2016), “Constitutive model for full-range elasto-plastic behavior of structural steels with yield plateau: calibration and validation”, *Eng. Struct*., **118**, 210-227. DOI: 10.1016/j.engstruct.2016.03.060.

Huang, Y. and Young, B. (2017), “Post-fire behaviour of ferritic stainless steel material”, *Constr. Build. Mater*., **157**, 654-67. DOI: 10.1016/j.conbuildmat.2017.09.082.

Jia, L.J. (2014), “Integration algorithm for a modified Yoshida–Uemori model to simulate cyclic plasticity in extremely large plastic strain ranges up to fracture”, *Comput. Struct*., **145**, 36-46. DOI: 10.1016/j.compstruc.2014.08.010.

Jia, L.J., Ge, H.B., Shinohara, K. and Kato, H. (2016), “Experimental and numerical study on ductile fracture of structural steels under combined shear and tension”, *J. Bridge Eng. -ASCE*, 04016008. DOI: 10.1061/(ASCE)BE.1943-5592.0000845.

Jia, L.J. and Kuwamura, H. (2015), “Ductile fracture model for structural steel under cyclic large strain loading”, *J. Constr. Steel Res*., **106**, 110-121. DOI: 10.1016/j.jcsr.2014.12.002.

Jia, L.J. and Kuwamura, H. (2014a), “Prediction of cyclic behaviors of mild steel at large plastic strain using coupon test results”, *J. Struct. Eng.- ASCE*, **140**(2), 04013056. DOI: 10.1061/(ASCE)ST.1943-541X.0000848.

Jia, L.J. and Kuwamura, H. (2014b), “Ductile fracture simulation of structural steels under monotonic tension”, *J. Struct. Eng.-ASCE*, **140**(5), 04013115. DOI: 10.1007/978-981-13-2661-5_4.

Jia, L.J., Ikai, T., Shinohara, K. and Ge, H.B. (2016), “Ductile crack initiation and propagation of structural steels under cyclic combined shear and normal stress loading”, *Constr. Build. Mater*., **112**, 69-83. DOI: 10.1016/j.conbuildmat.2016.02.171.

Kang, L., Ge, H.B. and Kato, T. (2015), “Experimental and ductile fracture model study of single-groove welded joints under monotonic loading”, *Eng. Struct*., **85**, 36-51. DOI: 10.1016/j.engstruct.2014.12.006.

Kang, L., Ge, H.B., Suzuki, M. and Wu, B. (2018), “An average weight whole-process method for predicting mechanical and ductile fracture performances of HSS Q690 after a fire”, *Constr. Build. Mater*., **191**, 1023-1041. DOI: 10.1016/j.conbuildmat.2018.10.068.

Kuhlmann-Wilsdorf, D. and Laird, C. (1979), “Dislocation behavior in fatigue II. Friction stress and back stress as inferred from an analysis of hysteresis loops”, *Mater. Sci. Eng*., **37**(2), 111-120. DOI: 10.1016/0025-5416(79)90074-0.

Liao, F., Wang, W. and Chen, Y. (2015), “Ductile fracture prediction for welded steel connections under monotonic loading based on micromechanical fracture criteria”, *Eng. Struct*., **94**, 16-28. DOI: 10.1016/j.engstruct.2015.03.038.

Mirambell, E. and Real, E. (2000), “On the calculation of deflections in structural stainless steel beams: an experimental and numerical investigation”, *J. Constr. Steel Res*., **54**(1), 109-133. DOI: 10.1016/S0143-974X(99)00051-6.

Ohno, N. (1982), “A Constitutive model of cyclic plasticity with a nonhardening strain region”, *J. Appl. Mech*., **49**(4), 721-727. DOI: 10.1115/1.3162603.

Quach, W.M., Teng, J.G. and Chung, K.F. (2008), “Three-stage full-range stress-strain model for stainless steels”, *J. Struct. Eng. - ASCE*, **134**(9), 1518-1527. DOI:10.1061/(asce)0733-9445(2008)134:9(1518).

Ramberg, W. and Osgood, W.R. (1943), “Description of stress-strain curves by three parameters”, National Advisory Committee for Aeronautics, Washington, D. C., USA.

Rasmussen, K.J.R. (2003), “Full-range stress–strain curves for stainless steel alloys”, *J. Constr. Steel Res*., **59**(1), 47-61. DOI: 10.1016/S0143-974X(02)00018-4.

Theofanous, M. and Gardner, L. (2009), “Testing and numerical modelling of lean duplex stainless steel hollow section columns”, *Eng. Struct*., **31**(12), 3047-3058. DOI: 10.1016/j.engstruct.2009.08.004.

Wang, X., Chen, X., Yan, M. and Chang, M. (2018), “Constitutive model for ratcheting behavior of Z2CND18.12N austenitic stainless steel under non-symmetric cyclic stress based on BP neural network”, *Steel Compos. Struct*., **28**(5), 517-525. 10.12989/scs.2018.28.5.517.

Wang, Y.Q., Chang, T., Shi, Y.J., Yuan, H.X., Yang, L. and Liao, D.F. (2014), “Experimental study on the constitutive relation of austenitic stainless steel S31608 under monotonic and cyclic loading”, *Thin-Wall. Struct*., **83**, 19-27. DOI: 10.1016/j.tws.2014.01.028.

Xiang, P., Shi, M., Jia, L.J., Wu, M. and Wang, C.L. (2018), “Constitutive model of aluminum under variable-amplitude cyclic loading and its application to buckling-restrained braces”, *J. Mater. Civ. Eng. - ASCE*, **30**(3), 04017304. DOI: 10.1061/(ASCE)MT.1943-5533.0002183.

Yin, F., Yang, L., Wang, M., Zong, L. and Chang, X. (2019), “Study on ultra-low cycle fatigue behavior of austenitic stainless steel”, *Thin-Wall. Struct*., **143**, 106205. DOI: 10.1016/j.tws.2019.106205.

Yousefi, A.M., Lim, J.B.P. and Clifton, G.C. (2018), “Cold-formed ferritic stainless steel unlipped channels with web perforations subject to web crippling under one-flange loadings”, *Constr. Build. Mater*., **191**, 713-725. DOI: 10.1016/j.conbuildmat.2018.09.152.

Yousefi, A.M., Uzzaman, A., Lim, J.B.P., Clifton, G.C. and Young, B. (2017), “Numerical investigation of web crippling strength in cold-formed stainless steel lipped channels with web openings subjected to interior-two-flange loading condition”, *Steel Compos. Struct*., **23**(3), 363-383. https://doi.org/10.12989/scs.2017.23.3.363.

Zhao, O., Rossi, B., Gardner, L. and Young, B. (2015), “Behaviour of structural stainless steel cross-sections under combined loading – Part I: Experimental study”, *Eng. Struct*., **89**, 236-46. DOI: 10.1016/j.engstruct.2014.11.014.

BU